INORGANIC CHEMISTRY

FRONTIERS

Accepted Manuscript

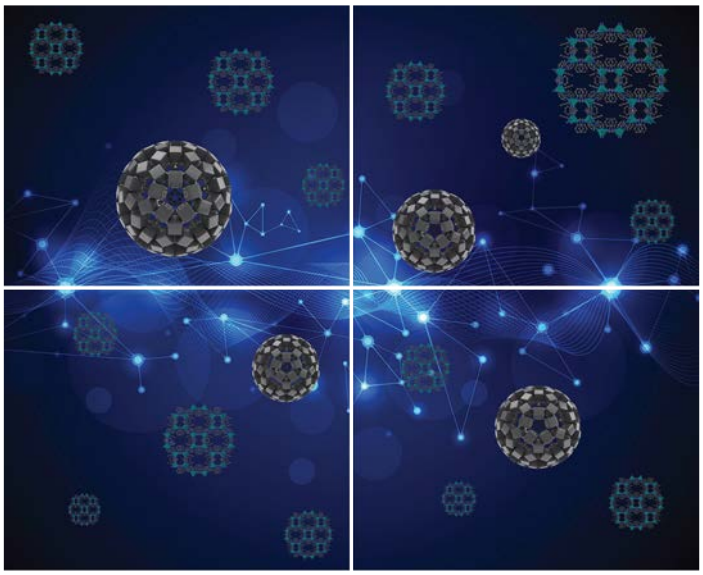

This article can be cited before page numbers have been issued, to do this please use: C. Bai, Y. Chu, J. Zhou, L. Wang, L. Luo, S. Pan and J. Li, *Inorg. Chem. Front.*, 2022, DOI: 10.1039/D1QI01251G.

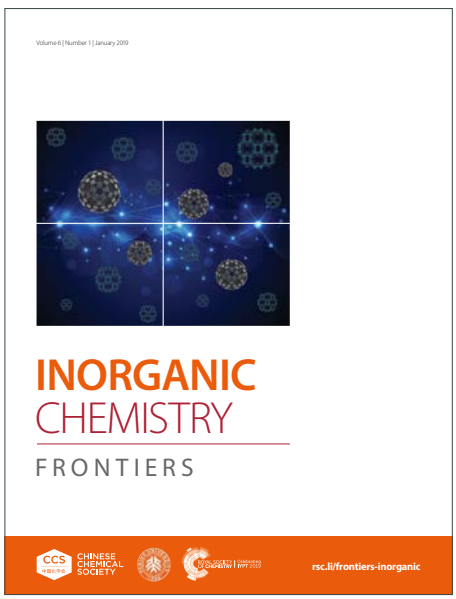

Inorganic Chemistry Frontiers

View Article Online
DOI: 10.1039/D1QI01251G

ARTICLE

Two New Tellurite Halides with Cationic Layers: Syntheses, Structures, and Characterizations of $CdPb_2Te_3O_8Cl_2$ and $Cd_{13}Pb_8Te_{14}O_{42}Cl_{14}$

Received 00th January 20xx,
Accepted 00th January 20xx

DOI: 10.1039/x0xx00000x-

Chen Bai,[#ab] Yu Chu,[#a] Jiazheng Zhou,[a] Linan Wang,[a] Ling Luo,[a] Shilie Pan*[a] and Junjie Li*[a]

Two new tellurite halides, $CdPb_2Te_3O_8Cl_2$ and $Cd_{13}Pb_8Te_{14}O_{42}Cl_{14}$ with cationic layer structures, have been synthesized by high-temperature solution method. $CdPb_2Te_3O_8Cl_2$ crystallizes in the noncentrosymmetric *Aba*2 space group, built by $[CdPb_2Te_3O_8]$ cationic layers with Cl atoms. $Cd_{13}Pb_8Te_{14}O_{42}Cl_{14}$ crystallizes in the centrosymmetric $P\bar{1}$ space group, constructed by $[Cd_{12}Pb_4Te_8O_{53}]$ layers, and $[Cd7Cl_6]$ octahedra as well as Cl atoms filled in the interlayers. In the two compounds, four unique oxyhalide mixed anionic groups, $[CdO_6Cl]$, $[PbO_3Cl_4]$, $[PbO_4Cl_4]$ and $[PbO_3Cl_5]$ were discovered. The experimental bands are ~3.89 eV for $CdPb_2Te_3O_8Cl_2$ and ~3.78 eV for $Cd_{13}Pb_8Te_{14}O_{42}Cl_{14}$. Furthermore, the powder second harmonic generation (SHG) response of $CdPb_2Te_3O_8Cl_2$ is about 0.2 × $AgGaS_2$ under 2029 nm (× 1.1 KDP @ 1064 nm), which is mainly originated from the triangular $[TeO_3]$ and distorted $[TeO_4]$ units. The results give an insight into the design of new IR optical materials by combing the heavy metal oxyhalide groups with the Te-O units.

Introduction

Inorganic tellurites have received considerable attentions recently, due to their promising applications in catalysis, ionic conductivity, magnetism, linear and non-linear optical (NLO) fields.[1-7] A known fact is that the physicochemical properties are dependent on the unique crystal structure of materials. Tellurium (IV) atom can be coordinated with 3-, 4- and 5-oxygen atoms to form TeO_3, TeO_4 and TeO_5 polyhedral units, which can be further interconnected to form various tellurium (IV) oxide, like one dimensional (1D) chains, two dimensional (2D) layers and three dimensional (3D) frameworks, showing abundant structural diversity and adjustable photoelectric properties.[8-11] Therefore, over the past decades, a great number of metal tellurites, like $MTeMoO_6$ (M = Cd, Mg, Zn),[12-14] $BaMo_2TeO_9$,[15] $Na_2W_2TeO_9$,[16] Bi_2TeO_5,[17] Co_3TeO_6,[18] $Li_2Ni_2TeO_6$,[6] Mg_3TeO_6,[19] $InNb(TeO_4)_2$,[20] $Hg_2Cu_3(Te_3O_8)_2$,[21] Li_2MTeO_6 (M = Ti, Sn),[22] and $Ba(MoO_2F)_2(QO_3)_2$(Q= Se, Te)[23] have been designed and fabricated.

To further increase the structural and functional diversity of metal tellurites, introducing the highly electronegative halogen atoms (e.g. F, Cl and Br) into tellurites has been demonstrated as a feasible way.[24] For example, Mao *et al.* reported the synthesis of $Li_7(TeO_3)_3F$ with a 3D anionic framework structure consisting of $[LiO_3F]$, $[LiO_4]$ and $[TeO_3]$ units by high-temperature solid-state reactions, showing potential applications in the fields of NLO and lithium battery.[25] Stolze and co-workers reported the synthesis of magnetic $CaCo_4(TeO_3)_4Cl_2$ with a layered structure built by $[CaO_8]$, $[CoO_5]$, $[CoO_3Cl]$ and $[TeO_3]$ units.[26] Berdonosov *et al.* reported the synthesis of luminophore activated $Na_2Ln_3Cl_3[TeO_3]_4$ (Ln = Sm, Eu, Gd, Tb, Dy and Ho) compounds with 3D anionic framework structure built by $[NaO_2Cl_4]$, $[LnO_8]$, $[LnO_9]$ and $[TeO_3]$ units.[27] What's more, compared with the light metal atoms, the bonding between heavy metal atoms and oxygen can effectively expand the infrared (IR) optical transmission regions of oxides (up to ~14 μm), indicating that the heavy metal oxyhalide could be a promising system for the development of new IR optical materials.[28]

In this work, combing the oxyhalide mixed anionic groups with Te-O units, two new tellurite halides, $CdPb_2Te_3O_8Cl_2$ and $Cd_{13}Pb_8Te_{14}O_{42}Cl_{14}$ were synthesized by high-temperature solution method. $CdPb_2Te_3O_8Cl_2$ and $Cd_{13}Pb_8Te_{14}O_{42}Cl_{14}$ crystallize in the noncentrosymmetric *Aba*2 (No. 41) and centrosymmetric $P\bar{1}$ (No.2) space groups, respectively. The 3D structures of the two compounds are composed of mixed cationic layer, with anions filling the interlayer to balance the charge. The experimental band gaps for $CdPb_2Te_3O_8Cl_2$ and $Cd_{13}Pb_8Te_{14}O_{42}Cl_{14}$ were ~3.89 and ~3.78 eV, respectively. The theoretical calculations indicate that the band gaps are mainly

[a] CAS Key Laboratory of Functional Materials and Devices for Special Environments; Xinjiang Technical Institute of Physics & Chemistry, CAS; Xinjiang Key Laboratory of Electronic Information Materials and Devices, 40-1 South Beijing Road, Urumqi 830011, China. E-mails: slpan@ms.xjb.ac.cn; lijunjie@ms.xjb.ac.cn
[b] College of Chemistry and Chemical Engineering, Xinjiang Normal University, 102 Xinyi Road, Urumqi 830054, China.
[#] These authors contributed equally to this work.

†Electronic Supplementary Information (ESI) available: Tables of crystal structure information; Selected Mulliken atomic populations of $CdPb_2Te_3O_8Cl_2$; Selected bond distances and Mulliken overlap populations for characteristic atomic pairs of $CdPb_2Te_3O_8Cl_2$; The EDS spectra of $CdPb_2Te_3O_8Cl_2$ and $Cd_{13}Pb_8Te_{14}O_{42}Cl_{14}$; Coordination of Cd1-Cd7 atoms; Te1-Te7 atoms and Pb1-Pb4 atoms in $Cd_{13}Pb_8Te_{14}O_{42}Cl_{14}$; Different coordination environments of $[CdO_nCl_m]$ and $[PbO_nCl_m]$; XRD patterns of $CdPb_2Te_3O_8Cl_2$ and $Cd_{13}Pb_8Te_{14}O_{42}Cl_{14}$ before and after heating at 550 and 650 °C respectively; SHG responses of $CdPb_2Te_3O_8Cl_2$ at 2.09 μm radiation; Calculated birefringence (Δn) of $CdPb_2Te_3O_8Cl_2$; SHG intensities of $CdPb_2Te_3O_8Cl_2$ and KDP as the references at 1064 nm radiation. CCDC $CdPb_2Te_3O_8Cl_2$: 2121770; CCDC $Cd_{13}Pb_8Te_{14}O_{42}Cl_{14}$: 2105596. see DOI: 10.1039/x0xx00000x

View Article Online
DOI: 10.1039/D1QI01251G

originated from the O 2*p*, Cl 3*p*, Te 5*p* and Pb 6*p* states in $[PbO_3Cl_4]$ and $[TeO_3]$ groups for $CdPb_2Te_3O_8Cl_2$, and O 2*p*, Cl 3*p*, Cd 4*p*, Te 5*p* states in $[Cd1O_6Cl_1]$ and $[TeO_3]$ units for $Cd_{13}Pb_8Te_{14}O_{42}Cl_{14}$. The powder SHG response of $CdPb_2Te_3O_8Cl_2$ is about 0.2 × $AgGaS_2$ under 2029 nm, and × 1.1 KDP under 1064 nm.

Experimental Section

Reagents

TeO_2 (99.99 %), $CdCl_2$ (99.99 %), $PbCl_2$ (99.90 %) and CdO (99.90 %) were purchased commercially and used as starting materials without further purification.

Chemical Syntheses

The single crystals of $CdPb_2Te_3O_8Cl_2$ and $Cd_{13}Pb_8Te_{14}O_{42}Cl_{14}$ for structural determination were obtained by high-temperature solution method. The molar ratio of starting materials is TeO_2 : $CdCl_2$: $PbCl_2$: CdO = 1 : 1 : 1 : 1. The reactants were mixed thoroughly in an agate mortar and then sealed in a quartz tube. The sample was heated to 550 °C and retained at this temperature for 24 h, and then decreased to 400 °C with a rate of 1 °C/h. Eventually, the furnace was turned off and the samples were cooled to room temperature naturally. It is worth noting that the two compounds were discovered simultaneously in the final products.

The pure phase polycrystalline powder samples of $CdPb_2Te_3O_8Cl_2$ and $Cd_{13}Pb_8Te_{14}O_{42}Cl_{14}$ were obtained by high-temperature solid-state reaction with different starting materials, $CdCl_2$: PbO : TeO_2 = 1 : 2 : 3 (molar ratio) for $CdPb_2Te_3O_8Cl_2$, and $CdCl_2$: PbO : CdO : TeO_2 = 7 : 8 : 6 : 14 (molar ratio) for $Cd_{13}Pb_8Te_{14}O_{42}Cl_{14}$. The mixtures were put into the graphite crucibles and sealed in quartz tubes. After that, the samples were slowly heated to 600 °C and held at this temperature for 24 h, and then cooled to room temperature at a rate of 2.4 °C/h.

Single-Crystal X-ray Diffractions (XRD)

The high-quality transparent single crystals were chosen for the structure determination. A Bruker SMART APEX II 4K CCD diffractometer with Mo Kα radiation (λ = 0.71073 Å) was used to collect the single-crystal XRD data of $CdPb_2Te_3O_8Cl_2$ and $Cd_{13}Pb_8Te_{14}O_{42}Cl_{14}$ at 296(2) K. The data were integrated with a SAINT program. The direct methods and SHELXTL system were used to solve and refine the crystal structures.[29] All of the atomic positions in the title compounds were refined by full-matrix least-squares techniques. After the structural determinations, no higher symmetries were found in the crystal structures. The detailed crystallographic data and structural refinements of $CdPb_2Te_3O_8Cl_2$ and $Cd_{13}Pb_8Te_{14}O_{42}Cl_{14}$ are listed in Table 1. The atomic coordinates, isotropic displacement parameters, bond valence sums, bond lengths and angles are presented in Tables S1–S2 for $CdPb_2Te_3O_8Cl_2$ and Tables S3–4S for $Cd_{13}Pb_8Te_{14}O_{42}Cl_{14}$.

Table 1. Crystal Data and Structure Refinements for $CdPb_2Te_3O_8Cl_2$ and $Cd_{13}Pb_8Te_{14}O_{42}Cl_{14}$.

Formula	$CdPb_2Te_3O_8Cl_2$	$Cd_{13}Pb_8Te_{14}O_{42}Cl_{14}$
Temperature	302.0 K	300.0 K
Wavelength	0.71073 Å	0.71073 Å
Crystal system	orthorhombic	triclinic
Space group, Z	*Aba*2, 4	$P\bar{1}$, 1
Unit cell dimensions	*a* = 18.2526(9) Å *b* = 8.1357(4) Å *c* = 7.9408(4) Å	*a* = 8.7487(4) Å *b* = 9.0158(4) Å *c* = 20.7187(9) Å α = 89.824(2) ° β = 84.919(2) ° γ = 89.158(2) °
Volume	1179.19 (10) Å^3	1627.62(13) Å^3
Density (calculated)	6.244 Mg / m^3	6.196 Mg / m^3
Absorption coefficient	38.018 mm^{-1}	31.558 mm^{-1}
F (000)	1864	2582
Theta range for data collection	2.232 to 27.553°	1.974 to 27.553°
Index ranges	-23 ≤ h ≤ 23 -10 ≤ k ≤ 10 -9 ≤ l ≤ 11	-11 ≤ h ≤ 11 -11 ≤ k ≤ 11 -26 ≤ l ≤ 26
Reflections collected	4579	65876
Independent reflections	1212	7518
Completeness	96%	99.90%
Flack index	0.011	-
Goodness-of-fit on F^2	1.123	1.106
Final R indices [I>2sigma(I)] [a]	R_1 = 0.0297, wR_2 = 0.0772	R_1 = 0.0423, wR_2 = 0.1098
R indices (all data) [a]	R_1 = 0.03, $wR2$ = 0.0775	R_1 = 0.0462, wR_2 = 0.1116

[a] $R_1 = \Sigma||F_o|-|F_c||/\Sigma|F_o|$ and $wR_2 = [\Sigma w(F_o^2 - F_c^2)^2/ \Sigma w F_o^4]^{1/2}$ for $F_o^2 > 2\sigma(F_o^2)$.

Powder XRD Analyses

The purities of the obtained powder samples for the title compounds were confirmed by powder X-ray diffraction (XRD), which was performed on a Bruker D2 PHASER diffractometer equipped with Cu Kα radiation at room temperature. The diffraction patterns were recorded from 5 to 80° (2θ ranges), with a scanning step width of 0.01° and a scanning rate of 1 s/ step.

Energy dispersive X-ray spectroscopy (EDS)

The EDS spectra of $CdPb_2Te_3O_8Cl_2$ and $Cd_{13}Pb_8Te_{14}O_{42}Cl_{14}$ were measured on crystals in a field emission scanning electron microscopy (FE-SEM, JEOL JSM-7610F Plus, Japan) with an energy dispersive X-ray spectroscopy (Oxford, X-Max 50), which was operated at 5 kV.

UV-Vis-NIR Diffuse-reflectance Spectra

To determine the absorption edge of $CdPb_2Te_3O_8Cl_2$ and $Cd_{13}Pb_8Te_{14}O_{42}Cl_{14}$, the UV−Vis−NIR diffuse reflectance spectra for $CdPb_2Te_3O_8Cl_2$ and $Cd_{13}Pb_8Te_{14}O_{42}Cl_{14}$ were characterized by a Shimadzu SolidSpec-3700 DUV spectrophotometer. Tetrafluoroethylene was used as the diffuse reflectance standard. The reflectance spectra were converted to

absorbance by the Kubelka–Munk function, $F(R) = (1-R)^2 / (2R)$, where R is the reflectance.[30]

Infrared (IR) Spectra

The infrared (IR) spectra of the title compounds were measured by Shimadzu IR Affinity-1 Fourier transform IR spectrometer. Before the measurements, the powder samples of $CdPb_2Te_3O_8Cl_2$ and $Cd_{13}Pb_8Te_{14}O_{42}Cl_{14}$ were mixed with dried KBr to prepare a thin sheet under pressure. The data were recorded in the range of 400-4000 cm^{-1}.

Powder SHG Measurement of $CdPb_2Te_3O_8Cl_2$.

For the second-order NLO materials, a noncentrosymmetric structure is essential. Since $CdPb_2Te_3O_8Cl_2$ crystallizes in the noncentrosymmetric *Aba*2 space group, the SHG responses of the compound were evaluated with the Kurtz-Perry method under ~1 μm and ~2 μm irradiations, respectively. For the measurement under 2090 nm, $AgGaS_2$ crystal powders were used as the references.[31-33] $CdPb_2Te_3O_8Cl_2$ and $AgGaS_2$ samples were ground and sifted into desired particle size ranges of 38-55, 55-88, 88-105, 105-150, and 150-200 μm and further poured into sample cells with a thickness of 1 mm. The measurement was implemented on a Q-switched laser (2090 nm, 50 ns, 1 Hz). A photomultiplier tube and Tektronix oscilloscope were used to detect and recorded the frequency-doubled intensity output from the samples.

For the measurement under 1064 nm, KDP crystal powders were used as the references. $CdPb_2Te_3O_8Cl_2$ and KDP samples were ground and sieved into distinct particle size ranges (55-88, 88-105, 105-150, 150-200, 200-250 μm). The samples were poured into sample cells and irradiated with a pulsed infrared beam produced by a Q-switched Nd:YAG laser at a wavelength of 1064 nm.

Thermal Analysis

The differential scanning calorimetry (DSC) curves were carried out on a NETZSCH STA 449F3 thermal analyzer instrument at a temperature range of 40–800 °C with a heating rate of 5 °C/min in an N_2 atmosphere.

First Principles Calculations

Theoretical calculations on the optical properties of the title compounds were performed based on the density functional theory (DFT) of the CASTEP package.[34] In the generalized gradient approximation (GGA),[35] the Perdew-Burke-Ernzerhof (PBE) function was used as the exchange-correlation function.[36,37] The band structures of the two compounds were firstly calculated at a kinetic energy cut-off of 910 eV with a separation of 0.04 $Å^{-1}$. To further confirm the band structure, a higher calculation accuracy (kinetic energy cut-off: 700 eV; separation 0.035 $Å^{-1}$) was used. To accurately evaluate the theoretical band gaps of the title compounds, the scissor operator was used.

Results and Discussion

Crystal Structure of $CdPb_2Te_3O_8Cl_2$

$CdPb_2Te_3O_8Cl_2$ crystallizes in the noncentrosymmetric *Aba*2 space group (No. 41) of orthorhombic crystal system with cell parameters a = 18.1555 (9) Å, b = 8.1514 (4) Å, c = 7.8801 (4) Å and Z = 4. In its asymmetric unit, there are one crystallographically unique Cd atom, one Pb atom, two Te atoms, four O atoms, and one chlorine atom. The EDX spectrum (Figure S1a) demonstrates the existence of Cd, Pb, Te, O and Cl elements in $CdPb_2Te_3O_8Cl_2$. The results of bond valence calculation in Table S1 indicate that the valence states of all atoms in $CdPb_2Te_3O_8Cl_2$ are in reasonable oxidation states.

The Cd1 atom is coordinated with eight O atoms to form $[CdO_8]$ polyhedra (Figure 1a) with Cd-O bond lengths of 2.334 - 2.642 Å. Pb1 is coordinated with three O atoms and four Cl atoms to form $[PbO_3Cl_4]$ polyhedra (Figure 1b) with Pb-O bond lengths of 2.299 - 2.363 Å and Pb-Cl bond lengths of 3.172 - 3.431 Å. Te1 is coordinated with three O atoms to form triangular $[Te1O_3]$ units (Figure 1c) with Te-O bond lengths of 1.872 - 1.896 Å, while Te2 is bonded to four O atoms to form twisted $[Te2O_4]$ polyhedral units (Figure 2d) with Te-O bond lengths of 1.908 - 2.141Å. The formed $[CdO_8]$ and $[PbO_3]$ units are isolated, which are connected with each other by shared oxygen atoms to form a $[CdPb_2O_8]$ layer (Figure 1e). The layer is further connected with $[TeO_3]$ and $[TeO_4]$ units by shared oxygen atoms to construct a complicate $[CdPb_2Te_3O_8]$ layer (Figure 1f). The $[CdPb_2Te_3O_8]$ layers are connected by Cl atoms

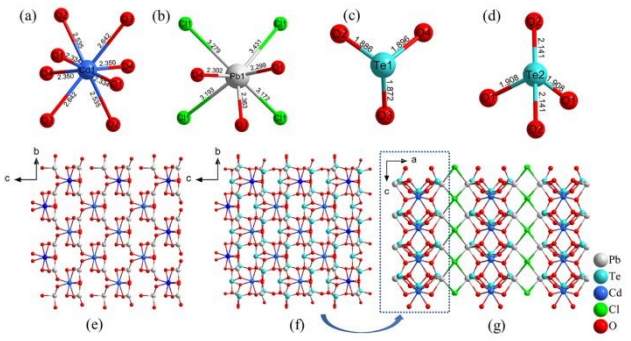

Figure 1. (a-d) Coordination modes of Cd1, Pb1, Te1 and Te2 atoms; (e)The structure of $[CdPb_2O_8]$ layer constructed by Isolated $[CdO_8]$ and $[PbO_3]$; (f)The structure of $[CdPb_2Te_3O_8]$ layer; (g) The three-dimensional framework structure of $CdPb_2Te_3O_8Cl_2$.

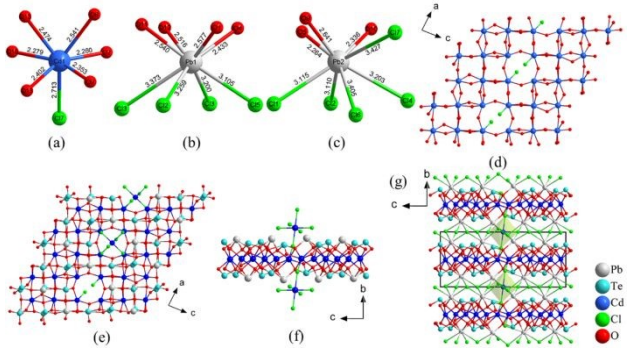

Figure 2. (a-c) Coordination modes of Cd1, Pb1 and Pb2 atoms; (d) The structure of $[Cd_{12}O_{45}Cl]$ layer; (e-f) The structure of $[Cd_{12}Pb_4Te_8O_{53}]$ layer viewed along the [010] and [100] directions, respectively; (g) The three-dimensional framework structure of $Cd_{13}Pb_8Te_{14}O_{42}Cl_{14}$.

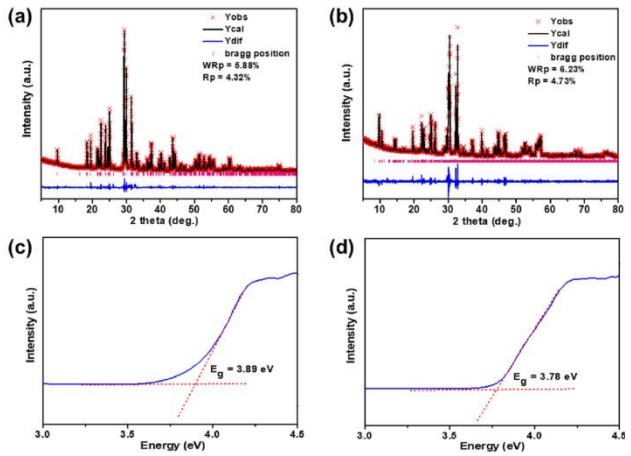

Figure 3. Rietveld refinements of PXRD and experimental band gaps of (a) (c) $CdPb_2Te_3O_8Cl_2$,(b) (d) $Cd_{13}Pb_8Te_{14}O_{42}Cl_{14}$.

to build the final 3D framework structure of $CdPb_2Te_3O_8Cl_2$, as shown in Figure 1g.

Crystal Structure of $Cd_{13}Pb_8Te_{14}O_{42}Cl_{14}$

$Cd_{13}Pb_8Te_{14}O_{42}Cl_{14}$ crystallizes in the centrosymmetric $P\bar{1}$ (No. 2) space group in the triclinic crystal system with cell parameters a = 8.7487(4) Å, b = 9.0158(4) Å, c = 20.7187 (9) Å , α = 89.824 (2) °, β = 84.919 (2) °, γ = 89.158 (2) ° and Z = 1. In the asymmetric unit, there are seven crystallographically unique Cd atoms, four Pb atoms, seven Te atoms, twenty-one O atoms and seven chlorine atoms, which shows more atoms than $CdPb_2Te_3O_8Cl_2$ in the unit. The EDX spectrum (Figure S1b) demonstrates the existence of Cd, Pb, Te, O and Cl elements in $Cd_{13}Pb_8Te_{14}O_{42}Cl_{14}$. The results of bond valence calculation (Table S3) indicate that the valence states of all atoms in $Cd_{13}Pb_8Te_{14}O_{42}Cl_{14}$ are in reasonable oxidation states.

As shown in Figure 2d, Cd1-Cd7 atoms are coordinated with O and/or Cl atoms to form the $[Cd1O_6Cl]$, $[Cd2O_7]$, $[Cd3O_6]$, $[Cd4O_8]$, $[Cd5O_6]$, $[Cd6O_8]$ and $[Cd7Cl_6]$ polyhedral units with Cd-O bond lengths of 2.141 - 2.858 Å and Cd-Cl bond length of 2.570 - 2.781 Å (Figure S2). Pb1-Pb4 atoms are coordinated with O and Cl atoms to form the $[Pb1O_4Cl_4]$, $[Pb2O_3Cl_5]$, $[Pb3O_3Cl_4]$ and $[Pb4O_3Cl_4]$ mixed anionic groups with Pb-O bond lengths of 2.264 - 2.695 Å and Pb-Cl band length of 3.105 - 3.405 Å, as shown in Figure S3. Different from the 3-fold and 4-fold coordinated Te atoms in $CdPb_2Te_3O_8Cl_2$, the seven crystallographically unique Te atoms in $Cd_{13}Pb_8Te_{14}O_{42}Cl_{14}$ are 3-fold coordinated with O to form the triangular $[TeO_3]$ units (Figure S4). The formed $[Cd1O_6Cl]$, $[Cd2O_8]$, $[Cd3O_6]$, $[Cd4O_8]$,

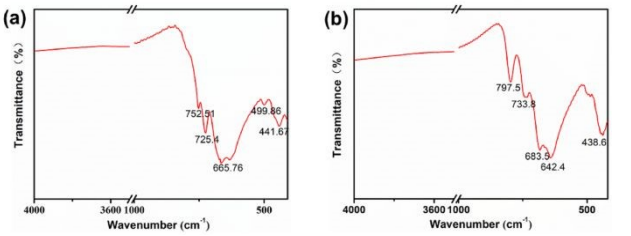

Figure 4. IR spectra of (a) $CdPb_2Te_3O_8Cl_2$ and (b) $Cd_{13}Pb_8Te_{14}O_{42}Cl_{14}$.

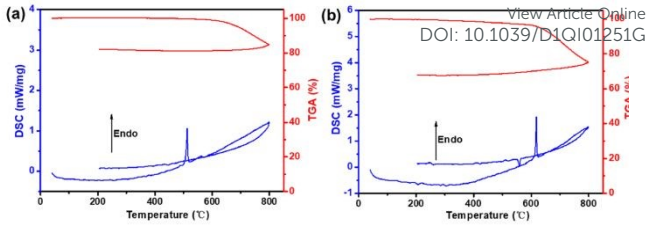

Figure 5. TGA and DSC curves of $CdPb_2Te_3O_8Cl_2$ (a) and $Cd_{13}Pb_8Te_{14}O_{42}Cl_{14}$ (b).

$[Cd5O_6]$ and $[Cd6O_8]$ polyhedral units are connected to form a layered $[Cd_{12}O_{45}Cl]$ structure by sharing oxygen atoms, as shown in Figure 2d. Then, the $[Cd_{12}O_{45}Cl]$ layer is further connected with the triangular $[TeO_3]$ and distorted $[Pb1O_4Cl_3]$, $[Pb2O_3Cl_5]$, $[Pb3O_3Cl_4]$ and $[Pb4O_4Cl_4]$ units to construct a $[Cd_{12}Pb_4Te_8O_{53}]$ layer (Figures 2e-2f). The resulted $[Cd_{12}Pb_4Te_8O_{53}]$ layers are connected with each other by sharing Cl atoms to build the final 3D framework, and the $[Cd7Cl_6]$ octahedral groups are located between the layers (Figure 2g).

In the two compounds, four unique oxyhalides mixed anionic groups were discovered. The formed $[CdO_6Cl]$ group in $CdPb_2Te_3O_8Cl_2$ is scarcely observed, which is different from the formed $[CdO_2Cl_4]$, $[CdO_3Cl_3]$, $[CdO_4Cl_2]$ and $[CdO_5Cl]$ mixed-anion groups in $C_3H_9Cd_{1.5}Cl_3O_4P$,[38] CdOHCl,[39] $Cd(IO_3)Cl$[40] and $Cd_5(BO_3)_3Cl$[41] (Figure S5). What's more, the formed $[PbO_3Cl_4]$, $[PbO_4Cl_4]$ and $[PbO_3Cl_5]$ units in the two compounds are different from the formed $[PbO_2Cl_2]$, $[PbO_2Cl_4]$, $[PbO_2Cl_3]$, $[PbOCl_5]$ and $[PbO_3Cl_3]$ mixed-anion groups (Figure S6) in $Pb_3O_2Cl_2$,[42] $Pb_{17}O_8Cl_{18}$,[28] $RbPb_8O_4Cl_9$[43] and $Ba_{27}Pb_8O_8Cl_{54}$.[44]

UV-Vis-NIR Diffuse Reflectance Spectra

To investigate the experimental band gaps of the title compounds, the pure phase of powder samples were synthesized and characterized. The powder XRD (PXRD) patterns and refined results in Figures 3a-3b confirmed the purity of the synthesized samples.[45] After that, the UV-Vis-NIR diffuse reflectance spectra were characterized on the basis of the pure phase powders. The absorption (K/S) data were depicted through the Kubelka-Munk function. As shown in Figures 4c-4d, The experimental band gaps are determined to 3.89 eV for $CdPb_2Te_3O_8Cl_2$ and 3.78 eV for $Cd_{13}Pb_8Te_{14}O_{42}Cl_{14}$, which are comparable to the ones in previously reported tellurite compounds like α-$CdTeO_3$ (3.91 eV),[46] and larger than the ones in $Pb_{17}O_8Cl_{18}$ (3.44 eV),[28] $Pb_{13}O_6Cl_4Br_{10}$ (3.05 eV),[47] $Pb_{13}O_6Cl_7Br_7$ (3.13 eV)[47] $Pb_{13}O_6Cl_9Br_5$ (3.21 eV)[47] $Pb_{18}O_8Cl_{15}I_5$ (2.82 eV)[48] and $CdPbOCl_2$ (3.63 eV)[49].

IR Spectra

To confirm the chemical bonding in the two compounds, the IR spectra were measured in the region from 400 to 4000 cm^{-1}. As shown in Figures 4a-4b, the characteristic absorption peaks at 665.76, 725.4 and 752.51 cm^{-1} for $CdPb_2Te_3O_8Cl_2$, and 642.4, 683.5, 733.8 and 797.5 cm^{-1} for $Cd_{13}Pb_8Te_{14}O_{42}Cl_{14}$ can be attributed to the Te-O stretching vibrations. The peaks at 441.67 and 499.86 cm^{-1}

for $CdPb_2Te_3O_8Cl_2$, and 438.6 cm^{-1} for $Cd_{13}Pb_8Te_{14}O_{42}Cl_{14}$ are related to the Te-O-Te vibrations.[21,50-54].

Thermal Analyses

To uncover the thermal stability of the title compounds, the TG-DSC experiments were carried out from room temperature to 800 °C. As shown in Figure 5, there is an obvious absorption peak at 512 °C for $CdPb_2Te_3O_8Cl_2$, and a peak at 618 °C for $Cd_{13}Pb_8Te_{14}O_{42}Cl_{14}$, accompanying with the weight loss starting at the temperatures in the TGA curves. To uncover the origin of the the temperatures in the TGA curves. To uncover the origin of the endothermic peaks, the synthesized pure phases $CdPb_2Te_3O_8Cl_2$ and $Cd_{13}Pb_8Te_{14}O_{42}Cl_{14}$ samples were heated to ~550 and ~650 °C, respectively. Based on the XRD patterns before and after heating (Figure S7), the endothermic peaks on the two DSC curves can be attributed to the decomposition of the two compounds. The thermal decomposition products could be $CdTe_3O_8$, PbO_4Cl_2 and Pb_2TeO_4 for $CdPb_2Te_3O_8Cl_2$, and Pb_3TeO_5 and Te_2O_5 for $Cd_{13}Pb_8Te_{14}O_{42}Cl_{14}$.

SHG Response of $CdPb_2Te_3O_8Cl_2$

$CdPb_2Te_3O_8Cl_2$ crystallizes in *mm*2 point symmetry, which has three independent SHG coefficients. The calculated SHG coefficients are d_{15} = 0.025, d_{24} = 1.587 and d_{33} = 0.9595 pm/V for $CdPb_2Te_3O_8Cl_2$. The powder SHG responses of $CdPb_2Te_3O_8Cl_2$ were investigated by the Kurtz and Perry method. The experimental results show that the powder SHG response is about 0.2 × $AgGaS_2$ at the size of 150-200 μm (Figure S8a) under 2090 nm, and × 1.1 KDP under 1064 nm (Figure S9).[55,56] However, the SHG intensities are not increased with the increase of particle sizes in the two measurements. It means that the compound is not in accordance with the type I phase-matching behavior due to its small birefringence of ~0.009 at 1064 nm (Figure S8b).[55-58] To detect the origin of SHG in the compound, the SHG density map of electron-including occupied and unoccupied states was calculated by DFT calculations (Figure 6). Meanwhile, the atomic populations (Tables S5-S6) and electron density maps (Figure S10) were further calculated and analyzed. The results indicate that the triangular $[TeO_3]$ and distorted $[TeO_4]$ units, with strong covalence Te-O bonding and lone pair electron effect, make the major contribution to the SHG responses. What's more, the calculated hyperpolarizabilities for $[TeO_3]$ and $[TeO_4]$ units are 3.65 and 8.79, respectively.

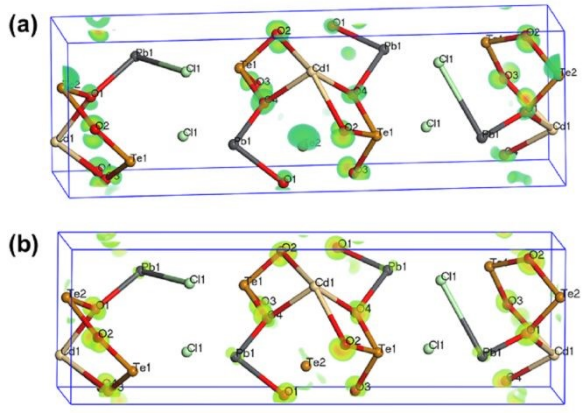

Figure 6. The SHG density of $CdPb_2Te_3O_8Cl_2$ at the occupied state (a), and at the unoccupied state (b).

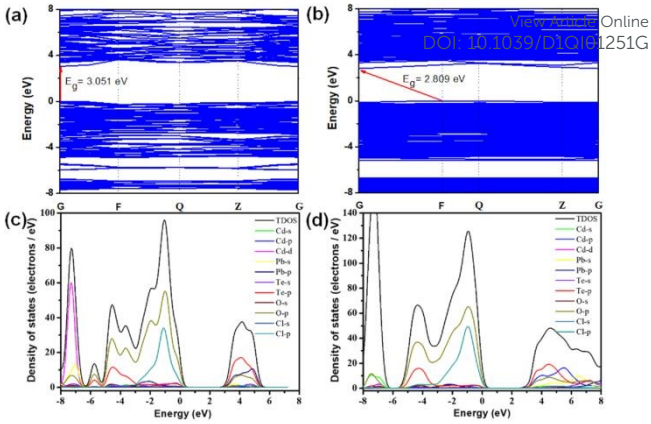

Figure 7. Band structures of (a) $CdPb_2Te_3O_8Cl_2$ and (b) $Cd_{13}Pb_8Te_{14}O_{42}Cl_{14}$; total and partial density of states of (c) $CdPb_2Te_3O_8Cl_2$ and (d) $Cd_{13}Pb_8Te_{14}O_{42}Cl_{14}$.

Band Structures

To clarify the origin of optical band gaps and the band structures, total and partial density of states (TDOS and PDOS) were studied for the two compounds by DFT calculations under different calculated accuracy (Figures 7 and S11). The calculated band gaps are ~3.0 eV (direct band gap) for $CdPb_2Te_3O_8Cl_2$ and ~2.8 eV (indirect band gap) for $Cd_{13}Pb_8Te_{14}O_{42}Cl_{14}$. The difference of band gap in the two compounds can attributed to their unique crystal structures. Moreover, in $CdPb_2Te_3O_8Cl_2$, the top of valence bands near the Fermi level is mainly filled with O 2*p* and Cl 3*p* states, and the bottom of conduction is mainly composed of O 2*p*, Te 5*p* and Pb 6*p* states, indicating that the band gap of $CdPb_2Te_3O_8Cl_2$ is mainly determined by the $[PbO_3Cl_4]$ and $[TeO_3]$ units. In $Cd_{13}Pb_8Te_{14}O_{42}Cl_{14}$, the top of valence bands near the Fermi level is mainly filled with O 2*p* and Cl 3*p* states, and the bottom of conduction is mainly composed of O 2*p*, Te 5*p* and Cd 4*p* states with a small mixture of Pb 6*s*, showing the main contribution of $[Cd1O_6Cl_1]$ and $[TeO_3]$ units on the band gap of $Cd_{13}Pb_8Te_{14}O_{42}Cl_{14}$.

Conclusions

In summary, the Cd-Pb-Te-O-Cl system has been investigated systematically in this work. Two tellurate halides, $CdPb_2Te_3O_8Cl_2$ and $Cd_{13}Pb_8Te_{14}O_{42}Cl_{14}$ have been synthesized by high-temperature solution method. $CdPb_2Te_3O_8Cl_2$ crystallizes with noncentrosymmetric *Aba*2 group, constructed by $[CdPb_2Te_3O_8]$ cationic layers and Cl atoms. The SHG responses of $CdPb_2Te_3O_8Cl_2$ are mainly originated from the triangular $[TeO_3]$ and distorted $[TeO_4]$ units. $Cd_{13}Pb_8Te_{14}O_{42}Cl_{14}$ crystallizes with centrosymmetric $P\bar{1}$ group, built by $[Cd_{12}Pb_4Te_8O_{53}]$ cationic layers, and $[Cd7Cl_6]$ octahedra and Cl atoms filling the interlayers. The experimental band gaps are ~3.89 eV for $CdPb_2Te_3O_8Cl_2$ and ~3.78 eV for $Cd_{13}Pb_8Te_{14}O_{42}Cl_{14}$, matched with the calculated results. What's more, the theoretical calculations indicate that the band gaps are mainly originated

from the O 2*p*, Cl 3*p*, Te 5*p* and Pb 6*p* states in $[PbO_3Cl_4]$ and $[TeO_3]$ groups for $CdPb_2Te_3O_8Cl_2$, and O 2*p*, Cl 3*p*, Cd 4*p*, Te 5*p* states in $[Cd1O_6Cl_1]$ and $[TeO_3]$ units for $Cd_{13}Pb_8Te_{14}O_{42}Cl_{14}$.

Conflicts of interest

There are no conflicts to declare

Acknowledgements

This work was supported by the S&T Partnership and International S&T Cooperation Program of Shanghai Cooperation Organization (2020E01040), High-level Talent Project of Xinjiang Uygur Autonomous Region (2020000039), National Natural Science Foundation of China (52002398,22122509), Xinjiang Key Laboratory of Electronic Information Materials and Devices (2017D04029).

References

1. G. Q. Shi, Y. Wang, F. F. Zhang, B. B. Zhang, Z. H. Yang, X. L. Hou, S. L. Pan and K. R. Poeppelmeier, Finding the next deep-ultraviolet nonlinear optical material: $NH_4B_4O_6F$, *J. Am. Chem. Soc.,* 2017, **139**, 10645-10648.
2. X. F. Wang, Y. Wang, B. B. Zhang, F. F. Zhang, Z. H. Yang and S. L. Pan, CsB_4O_6F: a congruent-melting deep-ultraviolet nonlinear optical material by combining superior functional units, *Angew. Chem. Int. Ed.,* 2017, **56**, 14119-14123.
3. B. B. Zhang, G. Q. Shi, Z. H. Yang, F. F. Zhang and S. L. Pan, Fluorooxoborates: beryllium-free deep-ultraviolet nonlinear optical materials without layered growth, *Angew. Chem. Int. Ed.,* 2017, **56**, 3916-3919.
4. M. Mutailipu, M. Zhang, B. B. Zhang, L. Y. Wang, Z. H. Yang, X. Zhou and S. L. Pan, $SrB_5O_7F_3$ functionalized with $[B_5O_9F_3]^{6-}$ chromophores: accelerating the rational design of deep-ultraviolet nonlinear optical materials, *Angew. Chem. Int. Ed.,* 2018, **57**, 6095-6099.
5. Y. Wang, B. B. Zhang, Z. H. Yang and S. L. Pan, Cation-tuned synthesis of fluorooxoborates: towards optimal deep-ultraviolet nonlinear optical materials, *Angew. Chem. Int. Ed.,* 2018, **57**, 2150-2154.
6. N. S. Grundish, I. D. Seymour, G. Henkelman and J. B. Goodenough, Electrochemical properties of three $Li_2Ni_2TeO_6$ structural polymorphs, *Chem. Mater.,* 2019, **31**, 9379-9388.
7. K. M. Ok, Functional layered materials with heavy metal lone pair cations, Pb^{2+}, Bi^{3+}, and Te^{4+}, *Chem. Commun.*, 2019, **55**, 12737-12748.
8. M. F. Lü, J. H. Jiang, B. Zhu, Y. W. Zhao, T. Y. Zhu, H. M. Yang, Y. Jin, H. Kabbour, K.-Y. Choi and W. T. A. Harrison, Lone-pair self-containment in pyritohedron-shaped closed cavities: optimized hydrothermal synthesis, structure, magnetism and lattice thermal conductivity of $Co_{15}F_2(TeO_3)_{14}$, *Dalton Trans.*, 2020, **49**, 2234-2243.
9. S. Konatham and K. Vidyasagar, Syntheses and structural characterization of vanado-tellurites and vanadyl-selenites: $SrVTeO_5(OH)$, $Cd_2V_2Te_2O_{11}$, $Ca_3VSe_4O_{13}{\cdot}H_2O$ and $Ba_2VSe_3O_{10}$, *J. Solid State Chem.,* 2017, **249**, 39-45.
10. M. J. Xia and R. K. Li, Structural variety in zinc telluro-phosphates: syntheses, crystal structures and characterizations of $Sr_2Zn_3Te_2P_2O_{14}$, $Pb_2Zn_3Te_2P_2O_{14}$ and $Ba_2Zn_2TeP_2O_{11}$, *Dalton Trans*., 2016, **45**, 7492-7499.
11. J. X. Xu, A. Assoud, N. Soheilnia, S. Derakhshan, H. L. Cuthbert, J. E. Greedan, M. H. Whangbo and H. Kleinke, Synthesis, structure, and magnetic properties of the layered copper (II) oxide $Na_2Cu_2TeO_6$, *Inorg. Chem.*, 2005, **44**, 5042-5046.
12. S. G. Zhao, X. X. Jiang, R. He, S. Q. Zhang, Z. H. Sun, J. H. Luo, Z. S. Lin and M. C. Hong, A combination of multiple chromophores enhances second-harmonic generation in a nonpolar noncentrosymmetric oxide: $CdTeMoO_6$, *J. Mater. Chem. C.,* 2013**,** ***1***, 2906-2912.
13. J. J. Zhang, Z. H. Zhang, Y. X. Sun, C. Q. Zhang, S. J. Zhang, Y. Liu and X. T. Tao, $MgTeMoO_6$: a neutral layered material showing strong second-harmonic generation, *J. Mater. Chem.,* 2012**, 22**, 9921-9927.
14. S. G. Zhao, J. H. Luo, P. Zhou, S.-Q. Zhang, Z. H. Sun and M. C. Hong, $ZnTeMoO_6$: a strong second-harmonic generation material originating from three types of asymmetric building units, *RSC Adv.,* 2013**, 3**, 14000-14006.
15. D. H. Yu, D. H. Sun, M. Avdeev, W. Qian, X. X. Tian, Q. F. Gu and X. T. Tao, New high-pressure polymorph of the nonlinear optical crystal $BaTeMo_2O_9$, *Cryst. Growth Des.,* 2015, **15**, 3110–3113.
16. J. Goodey, J. Broussard and P. S. Halasyamani, Synthesis, structure, and characterization of a new second-harmonic-generating tellurite: $Na_2TeW_2O_9$, *Chem. Mater.,* 2002, **14**, 3174-3180.
17. M. O. Kang, N. Bhuvanesh and P. S. Halasyamani, Bi_2TeO_5: synthesis, structure, and powder second harmonic generation properties, *Inorg. Chem.,* 2001, **40**, 1978-1980.
18. S. A. Ivanov, R. Tellgren, C. Ritter, P. Nordblad, R. Mathieu, G. André, N. V. Golubko, E. D. Politova and M. Weil. Temperature-dependent multi-k magnetic structure in multiferroic Co_3TeO_6, *Mater. Res. Bull.*, 2012, **47**, 63-72.
19. E. Selb, L. Declara, L. Bayarjargal, M. Podewitz, M. Tribus and G. Heymann, Crystal structure and properties of a UV-transparent high-pressure polymorph of Mg_3TeO_6 with second harmonic generation response, *Eur. J. Inorg. Chem.,* 2019, **43**, 4668-4676.
20. Y. H. Kim, W. D. Lee and M. O. Kang, Strong second harmonic generation (SHG) originating from combined second-order Jahn-Teller (SOJT) distortive cations in a new noncentrosymmetric tellurite, $InNb(TeO_4)_2$, *Inorg. Chem.,* 2014, **45**, 5240-5245.
21. X.-L. Cao, F. Kong, Z.-Z. He and J.-G. Mao, Structural and magnetic studies on three new mixed metal copper(ii) selenites and tellurites, *Dalton Trans.*, 2015, **44**, 11420-11428.
22. J. Choisnet, A. Rulmont and P. Tarte, Ordering phenomena in the $LiSbO_3$ type structure: the new mixed tellurates Li_2TiTeO_6 and Li_2SnTeO_6, *J. Solid State Chem.,* 1989, **82**, 272-278.
23. M.-L. Liang, Y.-X. Ma, C.-L. Hu, F. Kong and J.-G. Mao, $Ba(MoO_2F)_2(QO_3)_2$ (Q = Se, Te): partial fluorination of MoO_6 octahedra enabling two polar solids with strong and phase matchable SHG response, *Chem. Mater*., 2020, **32**, 9688-9695.
24. B. Zhu, J. H. Jiang, T. Y. Zhu, H. M. Yang, Y. Jin and M. F. Lü, Synthesis, crystal structures, and magnetic properties of one-dimensional alkali metal copper chlor-tellurites $A(NH_4)Cu_4Te_2O_6Cl_6$(A = K, Cs), $NaCu_4Te_2Cl_5O_6$ and $Rb_3(NH_4)_2Cu_{12}Te_6Cl_{16.5}O_{18}(OH)_{0.5}$, *Dalton Trans.,* 2020, **49**, 9751-9761.
25. J.-H. Feng, C.-L. Hu, H.-P. Xia, F. Kong and J.-G. Mao, $Li_7(TeO_3)_3F$: a lithium fluoride tellurite with large second harmonic generation responses and a short ultraviolet cutoff edge, *Inorg. Chem.,* 2017, **56**, 14697-14705.

26. K. Stolze, T. Kong, F. O. von Rohr and R. J. Cava, Crystal structure and anisotropic magnetic properties of $CaCo_4(TeO_3)_4Cl_2$, *J. Solid State Chem.,* 2018, **263**, 141-147.
27. D. O. Charkin, S. Zitzer, S. Greiner, S. G. Dorofeev, A. V. Olenev, P. S. Berdonosov, T. Schleid and V. A. Dolgikh, *Z. Anorg,* Synthesis, structures, and luminescent properties of sodium rare-earth metal (III) chloride oxotellurates(IV), $Na_2Ln_3Cl_3[TeO_3]_4$(Ln = Sm, Eu, Gd, Tb, Dy, and Ho), *Allg. Chem.,* 2017, **643**, 1654-1660.
28. H. Zhang, S. L. Pan, X. Y. Dong, Z. H. Yang, X. L. Hou, Z. Wang, K. B. Chang and K. R. Poeppelmeier, $Pb_{17}O_8Cl_{18}$: a promising IR nonlinear optical material with large laser damage threshold synthesized in an open system, *J. Am. Chem. Soc.,* 2015, **137**, 8360-8363.
29. G. M. Sheldrick, Crystal structure refinement with SHELXL, *Acta Crystallogr. C.,* 2015, **71**, 3-8.
30. J. Tauc, *Mater.* Absorption edge and internal electric fields in amorphous semiconductors, *Res. Bull.,* 1970, **5**, 721-729.
31. A. Abudurusuli, J. B. Huang, P. Wang, Z. H. Yang, S. L. Pan, and J. J. Li, $Li_4MgGe_2S_7$: the first alkali and alkaline-earth diamond-like infrared nonlinear optical material with exceptional large band gap, *Angew. Chem. Int. Ed.*, 2021, **60**, 24131–24136.
32. Y. Chu, P. Wang, H. Zeng, S. C. Cheng, X. Su, Z. H. Yang, J. J. Li and S. L. Pan, $Hg_3P_2S_8$: a new promising infrared nonlinear optical material with a large second-harmonic generation and a high laser-induced damage threshold, *Chem. Mater.* 2021, 33, 6514–6521.
33. D. J. Mei, W. Z. Cao, N. Z. Wang, X. X. Jiang, J. Zhao, W. K. Wang, J. H. Dang, S. Y. Zhang, Y. D. Wu, P. H. Rao and Z. S. Lin, Breaking through the "3.0 eV wall" of energy band gap in mid-infrared nonlinear optical rare earth chalcogenides by charge-transfer engineering, *Mater. Horiz.*, 2021, **8**, 2330-2334.
34. S. J. Clark, M. D. Segall, C. J. Pickard, P. J. Hasnip, M. J. Probert, K. Refson and M. C. Payne, First principles methods using CASTEP, *Z. Kristallogr*., 2005, **220**, 567-570.
35. J. P. Perdew, K. Burke and M. Ernzerhof, Generalized gradient approximation made simple, *Phys. Rev. Lett.,* 1996, **77**, 3865-3868.
36. J. S. Lin, A. Qteish, M. C. Payne and V. Heine, Optimized and transferable nonlocal separable ab initio pseudopotentials, *Phys. Rev. B.,* 1993, **47**, 4174-4180.
37. A. M. Rappe, K. M. Rabe, E. Kaxiras and J. D. Joannopoulos, Optimized pseudopotentials, *Phys. Rev. B.,* 1990, **41**, 1227-1230.
38. A. V. Anyushin, D. A. Mainichev, N. K. Moroz, P. A. Abramov, D. Y. Naumov, M. N. Sokolov, V. P. Fedin, Cd^{2+} complexation with $P(CH_2OH)_3$, $OP(CH_2OH)_3$, and $(HOCH_2)_2PO_2^-$: coordination in solution and coordination polymers, *Inorg. Chem.,* 2012, **51**, 9995-10003.
39. Y. Cudennec, A. Riou, Y. Gérault and A. Lecerf, Synthesis and crystal structures of Cd(OH)Cl and Cu(OH)Cl and relationship to brucite type, *J. Solid State Chem.,* 2000, **151**, 308-312.
40. B.-P. Yang and J.-G. Mao, Synthesis, crystal structure and optical properties of two new layered cadmium iodates: $Cd(IO_3)X$ (X=Cl, OH), *J. Solid State Chem.,* 2014, **219**, 185-190.
41. Y. X. Song, M. Luo, C. S. Lin, N. Ye, G. Y. Yan and Z. S. Lin, Experimental and *ab initio* studies of $Cd_5(BO_3)_3Cl$: the first cadmium borate chlorine NLO material with isolated BO_3 groups, *Dalton Trans.,* 2017, **46**, 15228-15234.
42. O. I. Siidra, S. V. Krivovichev, T. Armbruster and W. Depmeier, Crystal chemistry of the mendipite-type system $Pb_3O_2Cl_2$—$Pb_3O_2Br_2$, *Z. Kristallogr.,* 2008, **223**, 204-211.
43. Z. X. Fan, C. Bai, H. S. Shi, M. Zhang, B. Zhang, J. Zhang and J. J. Li, $RbPb_8O_4Cl_9$: the first alkali metal lead oxyhalide with distorted $[PbO_3Cl_3]$ and $[PbOCl_5]$ mixed-anion groups *Dalton Trans.,* 2021, **50**, 14038-14043.
44. Z. Li, X. X. Jiang, W. H. Xing, Z. S. Lin, J. Y. Yao and Y. C. Wu, Alkali-earth metal lead(ii) oxyhalide $Ba_{27}Pb_8O_8Cl_{54}$ exhibiting interesting $[Pb_4Ba_4O_4]^{8+}$ species, *New J. Chem.,* 2020, **44**, 1699-1702.
45. B. H. Toby, EXPGUI, a graphical user interface for GSAS, *J. Appl. Cryst.,* 2001, **34**, 210-213.
46. M. Poupon, N. Barrier, S. Petit and S. Boudin, A new β-$CdTeO_3$ polymorph with a structure related to α-$CdTeO_3$, *Dalton Trans.,* 2017, **46**, 1927-1935.
47. X. L. Chen, H. Jo and K. M. Ok, lead mixed oxyhalides satisfying all fundamental requirements for high-performance mid-infrared nonlinear optical materials, *Angew. Chem. Int. Ed.,* 2020, **132**, 7584-7590.
48. X. L. Chen, Q, Jing and K. M. Ok, $Pb_{18}O_8Cl_{15}I_5$: a polar lead mixed oxyhalide with unprecedented architecture and excellent infrared nonlinear optical properties, *Angew. Chem. Int. Ed.,* 2020, **132**, 20503-20507.
49. C. Bai, B. L. Cheng, K. W. Zhang, M. Zhang, S. L. Pan and J. J. Li, A new broad-band infrared window material CdPbOCl2 with excellent comprehensive properties, *Dalton Trans.,* 2020, **50**, 16401-16405.
50. T. A. Sullens and T. E. Albrecht-schmitt, Structure and properties of the thorium vanadyl tellurate, $Th(VO_2)_2(TeO_6)(H_2O)_2$, *Inorg. Chem.,* 2005, **44**, 2282-2286.
51. T. Sivakumar, K. M. Ok and P. S. Halasyamani, Synthesis, structure, and characterization of novel two- and three-dimensional vanadates: $Ba_{2.5}(VO_2)_3(SeO_3)_4{\cdot}H_2O$ and $La(VO_2)_3(TeO_6){\cdot}3H_2O$, *Inorg. Chem.,* 2006, **45**, 3602-3605.
52. M. K. Kim, S.-H. Kim, H.-Y Chang, P. S Halasyamani and K. M. Ok, New noncentrosymmetric tellurite phosphate material: synthesis, characterization, and calculations of $Te_2O(PO_4)_2$, *Inorg. Chem.,* 2010, **49**, 7028-7034.
53. D. W. Lee, S.-J. Oh, P. S Halasyamani and K. M. Ok, New quaternary tellurite and selenite: synthesis, structure, and characterization of centrosymmetric $InVTe_2O_8$ and Noncentrosymmetric $InVSe_2O_8$, *Inorg. Chem.,* 2011, **50**, 4473-4480.
54. S.-Y. Zhang, H.-L. Jiang, C.-F. Sun and J.-G. Mao, Syntheses, crystal structures, and properties of five new transition metal molybdenum (VI) selenites and tellurites, *Inorg. Chem.,* 2009, **48**, 11809-11820.
55. L. Kang, M. L. Zhou, J. Y. Yao, Z. S. Lin, Y. C. Wu and C. T. Chen, Metal thiophosphates with good mid-infrared nonlinear optical performances: a first-principles prediction and analysis, *J. Am. Chem. Soc.,* 2015, **137**, 13049-13059.
56. Y. Huang, L. Gao, H. H. Y, Z. H. Yang, J. J. Li and S. L. Pan, Na_6MQ_4 (M=Zn, Cd; Q=S, Se): Promising new ternary infrared nonlinear optical materials, *Chem. Eur. J.,* 2021, **27**, 6538-6544.
57. F. Liang, L. Kang, Z. S. Lin, Y. C. Wu and C. T. Chen, Analysis and prediction of mid-IR nonlinear optical metal sulfides with diamond-like structures, *Coord. Chem. Rev.*, 2017, **333**, 57-70.
58. P. F. Gong, F. Liang, L. Kang, X. G. Chen and Z. S. Lin, Recent advances and future perspectives on infrared nonlinear optical metal halides, *Coord. Chem. Rev.*, 2019, **380**, 83-102.